

Melt-processed all-polymer distributed Bragg reflector laser

Kenneth D. Singer^{1*}, Tomasz Kazmierczak², Joseph Lott², Hyunmin Song²,
Yeheng Wu¹, James Andrews³, Eric Baer², Anne Hiltner², and Christoph Weder²

¹Case Western Reserve University, Department of Physics, Cleveland, OH 44106

²Case Western Reserve University, Department of Macromolecular Science and Engineering, Cleveland, OH 44106

³Youngstown State University, Department of Physics and Astronomy, Youngstown, OH 44555

*Corresponding author: kenneth.singer@case.edu

Abstract: We have assembled and studied melt-processed all-polymer lasers comprising distributed Bragg reflectors that were fabricated in large sheets using a co-extrusion process and define the cavities for dye-doped compression-molded polymer gain core sheets. Distributed Bragg reflector (DBR) resonators consisting of 128 alternating poly(styrene) (PS) and poly(methyl methacrylate) (PMMA) layers were produced by multilayer co-extrusion. Gain media were fabricated by compression-molding thermoplastic host polymers doped with organic laser dyes. Both processing methods can be used in high-throughput roll-to-roll manufacturing. Optically pumped DBR lasers assembled from these components display single and multimode lasing in the reflection band of the resonators, with a slope efficiency of nearly 19% and lasing thresholds as low as $90\mu\text{J}/\text{cm}^2$. The lasing wavelength can be controlled via the layer thickness of the DBR resonator films, and variation of the laser dye. Studies of threshold and efficiency are in agreement with models for end-pumped lasers.

© 2008 Optical Society of America

OCIS codes: (140.7260) Vertical cavity surface emitting lasers ; (160.5470) Polymers ; (140.2050) Dye lasers

References and links

1. I.D.W. Samuel, "Fantastic plastic," *Nature* **429**, 709-711 (2004).
2. I.D.W. Samuel and G.A. Turnbull, "Organic semiconductor lasers," *Chem. Rev.* **107**, 1272-1295 (2007).
3. P.K.H. Ho, D.S. Thomas, R.H. Friend, and N. Tessler, "All-polymer optoelectronic devices," *Science* **285**, 233-236 (1999).
4. S. W. Kim, S. S. Oh, J. H. Park, E. H. Choi, Y. H. Seo, G. S. Cho, and B. Park, "One-dimensional birefringent photonic crystal laser," *J. Appl. Phys.* **103**, 033103 (2008).
5. C. Kallinger, M. Hilmer, A. Haugeneder, M. Perner, W. Spirkl, U. Lemmer, J. Feldmann, U. Scherf, K. Mullen, A. Gombert, and V. Wittwer, "A flexible conjugated polymer laser," *Adv. Mater.* **10**, 920-923 (1998).
6. S.Y. Chou, P.R. Krauss, and P.J. Renstrom, "Imprint of sub-25 nm vias and trenches in polymers," *Appl. Phys. Lett.* **67**, 3114-3116 (1995).
7. M. Berggren, A. Dodabalapur, and R.E. Slusher, "Organic solid-state lasers with imprinted gratings on plastic substrates," *Appl. Phys. Lett.* **72**, 410-411 (1998).
8. A. Roger, M. Meier, A. Dodabalapur, E.J. Laskowski, and M.A. Capuzzo, "Distributed feedback ridge waveguide lasers fabricated by nanoscale printing and molding on nonplanar substrates," *Appl. Phys. Lett.* **64**, 3257-3259 (1999).
9. T. Komikado, S. Yoshida, and S. Umegaki, "Surface-emitting distributed-feedback dye laser of a polymeric multilayer fabricated by spin coating," *Appl. Phys. Lett.* **89**, 061123 (2006).
10. J. Yoon, W. Lee, J. M. Caruge, M. Bawendi, E. L. Thomas, S. Kooi, and P. N. Prasad, "Defect-mode mirrorless lasing in dye-doped organic/inorganic hybrid one-dimensional photonic crystal," *Appl. Phys. Lett.* **88**, 091102 (2006).

11. H. Takeuchi, K. Natsume, S. Suzuki, and H. Sakata, "Microcavity distributed-feedback laser using dye-doped polymeric thin films," *Electron. Lett.* **43**, 30-32 (2007).
12. T. Kazmierczak, H. Song, A. Hiltner, and E. Baer, "Polymeric one-dimensional photonic crystals by continuous coextrusion," *Macromol. Rapid Commun.* **28**, 2210-2216 (2007).
13. C. Löwe and C. Weder, "Synthesis and properties of photoluminescent 1,4-bis-(α -cyano-4-methoxystyryl)-benzenes," *Synthesis Sp.Is.* **(9)** 1185-1190 (2002).
14. B. Crenshaw and C. Weder, "Thermally induced color changes in melt-processed photoluminescent polymer blends," *Adv. Mater.* **17**, 1471-1476 (2005).
15. P. W. Milonni and J. H. Eberly, *Lasers* (John Wiley & Sons, 1991).

1. Introduction

Polymer-containing lasers attract significant attention because of the broad tailorability and potential processing advantages of polymers.[1] A major reason for the widespread interest in lasers that comprise either polymeric gain media, polymeric resonators, or both, is the relative processing ease of polymeric materials vis á vis inorganic semiconductors.[2] The possibility to fabricate all-polymer lasers through plastic fabrication processes is particularly attractive.[3,4] However, because polymer resonators involve periodic microstructures, the vast majority of organic lasers reported in the literature require comparably complex fabrication processes, for example embossing,[5] (nano)imprinting,[6] conventional or soft lithography,[7,8] or repetitive spin-coating.[9,10,11] Recently, a distributed Bragg reflector (DBR) laser having commercial multilayer film reflectors was reported.[4] This report describes the fabrication of surface-emitting DBR lasers, which consist of a compression-molded dye-doped polymer gain medium and photonic crystal (PC) resonators fabricated by multilayer polymer co-extrusion.[12] By careful design and process optimization, outstanding performance has been achieved. Both processing methods involve simple shaping of melted polymers and lend themselves to high-throughput roll-to-roll manufacturing of all plastic lasers. The resulting lasers can be mass produced and could find application in spectroscopy, remote sensing, data storage, and display.

2. Materials and Processing

The resonators (Fig. 1(a)) were fabricated by a layer-multiplying co-extrusion process (Fig. 1(b),(c)), [12] and consisted of 128 alternating layers of poly(methyl methacrylate) (PMMA) and polystyrene (PS). The process involves feeding the polymer melts into a coextrusion feedblock and then into a series of six multiplying elements (Fig. 1(b)), each of which slices the melt vertically, spreads it horizontally and recombines it to double the number of layers. A removable polyethylene skin layer is applied just before the exit die in order to smooth the

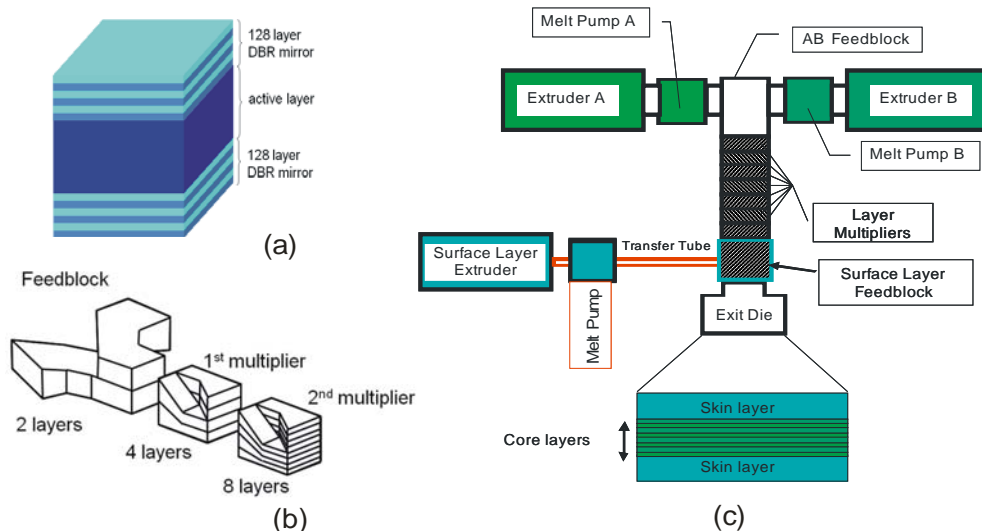


Fig. 1. (a) Distributed Bragg reflector laser structure. (b) Layer multiplier schematic. (c) Multilayer coextrusion process.

spreading forces in the exit die resulting in a more uniform film and higher quality reflection band. The difference of the refractive indices n of PS ($n=1.585\pm 0.002$) and PMMA ($n=1.489\pm 0.002$) causes the multilayer films to display a sharp reflection band. The centers of the resonators' reflection bands were matched with the emission spectra of two series of gain media by controlling the thickness of the polymer layers during the extrusion process, and fine-tuning the properties by reducing the film thickness by subsequent biaxial stretching.[12] The layers thicknesses were designed so that the high energy edge of the reflection band coincided with the emission maximum of the laser dye.

Gain media were prepared by incorporating the fluorescent organic dyes rhodamine 6G perchlorate (R6G) (with molecular weight, MW=546 g/mole) and 1,4-bis-(α -cyano-4-methoxystyryl)-2,5-dimethoxy-benzene[13] (C1-RG, Fig. 2(a)) (with molecular weight, MW=452 g/mole) into glassy amorphous host polymers and compression-molding thin films whose thickness was varied between 10 and 137 μm . C1-RG is highly soluble in PMMA[14] and C1-RG/PMMA blends (1.6×10^{-3} to 5.3×10^{-2} M) display strong green fluorescence and a large Stokes shift with absorption (λ_a) and emission (λ_e) maxima of ~ 430 and ~ 501 nm (Fig. 2(a)). The R6G/PMMA blends (3.3×10^{-4} to 1.0×10^{-2} M) display a smaller Stokes shift ($\lambda_a=532$ nm; $\lambda_e=565$ nm) (Fig. 2(b)) than C1-RG/PMMA and were photochemically more stable. Lasers were assembled by sandwiching two DBR mirrors (with reflection bands matched to the emission maxima of the gain medium) and the gain medium between two glass slides; a minute amount of silicon oil was applied to all interfaces as an index-matching fluid. For R6G lasers, the layer thicknesses of the reflectors were approximately 92 ± 21 nm yielding a band center at 565 nm. In the case of C1-RG lasers the layer thicknesses of the reflectors were approximately 84 ± 19 nm resulting in a band center at 510 nm. In order to minimize fluctuations in the layer thickness and ease manufacture, a 50:50 feedblock was employed giving each single layer approximately the same thickness. Fig. 2 shows the absorption and emission spectra of the dye as well as the transmission spectrum of the multilayer films.

3. Experimental

Refractive indices were measured at 633 nm with a Metricon 2010TM prism coupler. The fluorescence spectra were recorded with an ICCD camera spectrometer with excitation at 430nm (C1-RG) or 532nm (R6G). The surface-emitting lasers were pumped at oblique incidence with a tunable optical parametric oscillator (OPO), which was pumped by a frequency-tripled Nd:YAG laser ($\lambda = 355$ nm, pulse length 7 ns, frequency 10 Hz, p-polarized). Lasers comprising R6G and C1-RG gain media were pumped at 530 nm, and 430 nm, respectively. A rotatable half-wave plate together with a linear polarizer was used to control the power of the incident beam in a continuous manner. The pump beam, focused by a lens with 7.5 cm focal length, was incident at an angle of 10° from normal, allowing the pump light to fully penetrate the DBR reflectors by avoiding the reflection band. A knife-edge

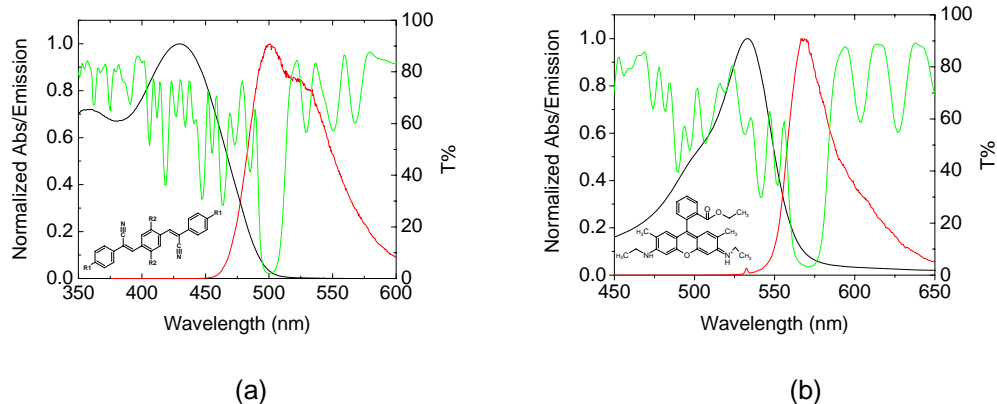


Fig. 2. a) Reflection band (green), absorption (black) and emission (red) of C1-RG (inset shows molecular structure) b) Reflection band (green), absorption (black) and emission (red) of R6G

technique was used to measure the spot size of the focused pump beam. An objective lens was employed to collect the emission at the normal direction. Color filters were used to block the scattered pump light. An ICCD camera spectrometer was used to measure the emitted spectrum, and calibrated photodiodes were employed to measure the input and output power.

4. Results

The DBR mirrors comprising 128 alternating PS and PMMA layers (i.e., 64 each) had a standard deviation of layers thickness of 22% and a film thickness of about 10 -12 μm as determined by direct measurement of AFM images of the film cross section. This non-uniformity results in the appearance of relatively intense and irregular side peaks, as is evident in Fig. 2(a) and (b). Intense laser emission was observed from all devices as can be seen from the picture shown in Fig. 3(a). Note the high quality emission mode. The minimum threshold fluence observed in C1-RG samples was 435 $\mu\text{J}/\text{cm}^2$ in a laser having a 135 μm thick gain layer comprising the dye in a concentration of 1.6×10^{-3} M, In the case of R6G lasers, the minimum threshold fluence was 90 $\mu\text{J}/\text{cm}^2$ in a device having a 40 μm thick gain layer at 5.4×10^{-3} M. The laser output in C1-RG samples decayed over several hours of service. The decay mechanism is currently under investigation. Interestingly, the output of the R6G samples was stable over long periods of time, which bodes well for the potential technological application of these devices.

Typical emission spectra both below and above threshold for DBR laser samples are shown in Fig. 4(a). Multimode emission was observed with the number of modes and spacing, of course, depending on the film thickness. Emission near the band center is as expected. The spectral width (full width half maximum) of a single lasing mode is about 0.4nm, near the instrumental resolution. The emission spectra of the photoluminescent dyes employed are rather broad with distinct phonon modes, as shown in Fig. 2. By contrast, the emission spectra of the DBR devices pumped below the lasing threshold are more complex and include contributions that arise from the reflection of the multilayer film and also periodic oscillations as shown in Fig. 4(a) (black curve). The oscillations are due to interference effects associated with DBR cavity reflection, and are indicative of the cavity modes.

We also characterized the energy conversion efficiency of the lasers studied. A typical plot of output power in the forward direction versus input power is shown in Fig. 3(b). The slope efficiency for this sample is 14.3%. The highest efficiency observed for C1RG lasers was 14.3% in a device having a 120 μm PMMA thick gain layer doped with 1.3×10^{-2} M dye. The highest efficiency we observed was 19.3% for a R6G sample having a 40 μm PMMA core

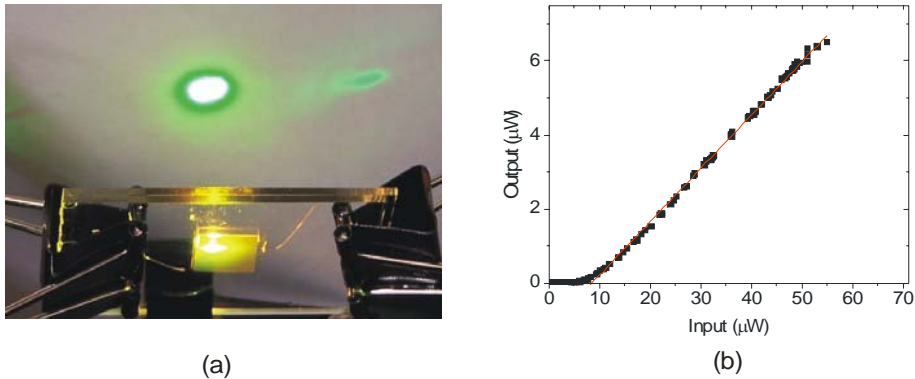


Fig. 3. (a) Bright emission from R6G DBR laser. The saturated bright spot on the screen (yellowish green) is the lasing emission and the fainter green spot to the right is the residue of the pump light. (b) Slope efficiency (14.3%) of a C1RG laser with 120 mm thick gain layer at 1.3×10^{-2} M in PMMA.

layer doped with 5.4×10^{-3} M dye.

The lasing thresholds as a function of thickness for R6G films having a gain medium doped at 5.4×10^{-3} M are shown in Fig. 4(b). The relatively large uncertainties are due to sample to sample variations, as well as variations across the sample surface of the DBR films that are correspondingly due to variations in the layer thicknesses across the surface as noted above. For each sample, results were averaged over several spots on the surface. Despite the uncertainties, it is obvious from Fig. 4(b) that R6G lasers comprising a gain medium doped with 5.4×10^{-3} M dye exhibit a threshold minimum when the core thickness is about 25 μm . This corresponds to an optical density (O.D.) of about 1.1. For lasers containing either R6G or C1-RG doped gain media of various dye concentrations, the minimum threshold was observed to be in the 1.1-1.4 O.D. indicating this is a generally favorable design criterion.

The dye lasers investigated here can be quantitatively described by a 4-level end-pumped laser model including re-absorption and scattering of the laser output, as well as the case of non-uniform pumping in an absorbing gain medium. For steady-state lasing, the threshold gain, g_{th} , can be expressed by: [15]

$$g_{th} = -\frac{1}{2l} \ln(r_1 r_2) + a \quad (1)$$

where l is the length of the gain medium, r_1, r_2 are the reflectivities of the two mirrors and a is the general loss at the lasing wavelength (arising from absorption, collision, scattering, etc) in the cavity. This expression reflects that a device with thinner gain medium should have higher threshold gain requiring a higher pump intensity. Further, the required minimum population inversion ΔN_{th} is determined by g_{th} and the stimulated emission cross section $\sigma(\omega)$. In a four-level system, the population inversion is proportional to pumping density.

$$\Delta N_{th} = g_{th} / \sigma(\omega) \quad (2)$$

Considering the case where the pumping is nonuniform, i.e. when the absorption is sufficiently high so that the pump intensity attenuates over the thickness of the active core, the threshold power, P_{th} , can then be expressed as,

$$\frac{P_{th}(1 - e^{-\alpha l})}{V} \approx \hbar \omega \Delta N_{th} \Gamma_{e'g'} \quad (3)$$

where α is the absorption coefficient at the pump wavelength, V the volume of the gain medium, which, in the low attenuation limit, equals the product of the spot area S and the length of the gain medium l . $\Gamma_{e'g'}$ is the transition rate from e' to g' , the lasing transitions. In

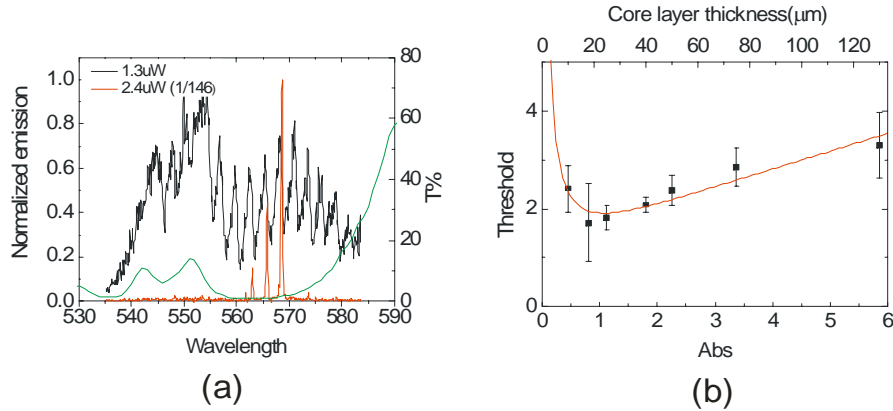


Fig. 4. (a) Emission spectrum of a R6G sample pumped below threshold (black curve) and above threshold (red). Transmission curve of the whole sample is shown as the green curve. (b) Threshold trend observed on R6G samples. Data points were fitted by a 4-level lasing model (Eq. 4), solid curve (red).

the left hand side of Eq. (3), the average pump density was used. Therefore, with Eqs. (1-3), we can express the pump threshold P_{th} by,

$$P_{th} \sim \frac{K(-\ln(r_1 r_2) + 2(\alpha l)a / \alpha)}{1 - e^{-\alpha l}} \quad (4)$$

In Eq. (4), K is a constant determined only by the type of molecule and the focusing of the pump beam.

The trend of the data shown in Fig. 4(b) is fully consistent with Eq. (4). The observed trends can be explained in the following way. In thin gain media layers, the dye molecules were efficiently excited throughout. However, the overall gain is small because most of the pump light is not absorbed by dye molecules while the loss due to the reflectors is fixed. As a result, a high pump threshold was observed for the thin gain layer samples. However, for lasers with thicker gain layers, the pump light penetration is limited by absorption, which implies an effective gain thickness smaller than the physical thickness, and, consequently, nonuniform pumping. In addition, re-absorption of the laser output by the dye molecules in lasers with thicker gain layers reduces the output. Both of these effects tend to increase the threshold in thicker lasers with thicker gain layers.

Equation (4) further implies that, for a specific dye concentration, there is an optimum absorption at which the device exhibits a minimum lasing threshold. The optimized absorption is determined by the output coupling and the ratio of loss to pump efficiency, described by a/α . For example, consider the system we studied, typical value of $r_1 r_2$ would be around 0.9 and $a/\alpha \sim 0.005$, if we only consider the absorption loss from the dye molecule itself. Then the optimized absorption would be 1.13 OD. It should be noted that Eq. (4) implies that the optimized absorption increases when the $r_1 r_2$ increases or a/α decreases. If the dye concentration in the polymer film is increased, since the scattering and collision losses from the polymer host do not change, a/α will become smaller. As a result, the optimized absorption is larger for higher concentration film. We have plotted Eq. (4) with K adjusted to fit the data, and the other parameters estimated from transmission data. The theory and data are in reasonable agreement.

In summary, we have described all-polymer surface emitting micro-resonator dye lasers with distributed Bragg reflectors. These lasers are produced entirely by melt-processes that lend themselves to high-throughput roll-to-roll production methods. Low threshold, high efficiency lasers having well-defined spatial and temporal modes were observed. Threshold measurements for lasers of various thickness and dye concentration were consistent with a simple four-level lasing model including inhomogeneous end-pumping and re-absorption.

Acknowledgements

The authors are grateful to the National Science Foundation for financial support under the Science and Technology Center for Layered Polymer Systems under grant number 0423914.